

Intrinsic Instability of Aberration-Corrected Electron Microscopes

S.M. Schramm¹, S.J. van der Molen¹, and R.M. Tromp^{1,2}

¹Leiden University, Kamerlingh Onnes Laboratorium,
P.O. Box 9504, NL-2300 RA Leiden, The Netherlands

²IBM T.J. Watson Research Center, 1101 Kitchawan Road, P.O. Box 218,
Yorktown Heights, NY 10598, USA

Aberration-corrected microscopes with sub-atomic resolution will impact broad areas of science and technology. However, the experimentally observed lifetime of the corrected state is just a few minutes. Here we show that the corrected state is intrinsically unstable; the higher its quality, the more unstable it is. Analyzing the Contrast Transfer Function near optimum correction, we define an ‘instability budget’ which allows a rational trade-off between resolution and stability. Unless control systems are developed to overcome these challenges, intrinsic instability poses a fundamental limit to the resolution practically achievable in the electron microscope.

Correction of spherical and chromatic aberrations of the electron microscope constitutes one of the most far-reaching breakthroughs in electron optics in the last 20 years¹. Now, Transmission Electron Microscopy (TEM) with 50 pm resolution provides a detailed view of carbon atoms in a single sheet of graphene². The resolution of Low Energy Electron Microscopy (LEEM) has improved³ from 5-10 nm to below 2 nm, with a theoretical limit of ~ 1 nm, opening up new possibilities for the dynamic imaging of surfaces, interfaces and thin films, including domain boundaries and domain walls, as well as nanometer-scale organic and biological materials. Photo Electron Emission Microscopy (PEEM), uniquely suited for elemental, chemical, electronic, and magnetic imaging, has achieved⁴ ~5 nm resolution, with a further factor 2 improvement still possible. Aberration correction has also been applied to Scanning Electron Microscopy (SEM)⁵ and Focused Ion Beam (FIB)⁶ systems, and is being considered for applications in semiconductor electron beam lithography and inspection tools⁷. Reduction of electron energy while maintaining atomic resolution will drastically reduce radiation damage in delicate organic and biological samples⁸. Undoubtedly, this revolutionary technology will impact many areas of science and technology, including physics, chemistry, materials science, geology, archeology, biology, medicine, manufacturing, etcetera. However, significant unresolved issues still remain. Recent experience with TEM shows that the optimum corrected state can be maintained for only a few minutes, after which the microscope drifts away and must be re-adjusted⁹⁻¹¹, a serious concern to microscope designers and users alike.

Here we discuss how resolution depends on the degree to which aberrations are corrected: resolution is exquisitely sensitive to small deviations from full correction, and

is intrinsically unstable against small fluctuations. For instance, to achieve at least 90% of the resolution improvement afforded by correction of the 3rd order spherical aberration coefficient C_3 , with simultaneous correction of the chromatic aberration coefficient C_c , C_3 must be corrected to within 1/10,000th of its uncorrected value. For a typical TEM with $C_3 = 1$ mm, correction must therefore be accurate and stable to within 0.1 μm . Correction of the 5th order spherical aberration C_5 , in addition to C_c and C_3 , is even harder, and it appears unlikely that a stable state could be maintained for any significant length of time. Aberration correction may utilize either axially symmetric electron mirrors¹² as in LEEM/PEEM, or sophisticated multipole optics¹³ as in (Scanning) TEM. That such aberration-corrected TEM instruments have stringent environmental and electronic stability requirements is well documented¹⁴. However, the fact that corrected electron optical instruments are *intrinsically unstable* does not appear to be widely recognized or appreciated.

In the simplest approach we define the resolution, δ , as follows:

$$\delta^2 = (0.61\lambda/\alpha)^2 + (C_c \alpha)^2 + (C_3 \alpha^3)^2 + (C_5 \alpha^5)^2 + \dots \quad (1)$$

where λ is the electron wavelength, and α the normalized energy spread $\Delta E/E$. The first term, $0.61\lambda/\alpha$, is the Rayleigh limit, due to a contrast aperture with angular range $\pm \alpha$. The best resolution occurs when $d\delta/d\alpha = 0$. We consider three limiting cases in which two aberration coefficients are set to zero, and the third is free to vary, leading to the following power-laws:

$$\begin{aligned} C_3 = C_5 = 0: & \quad \delta \propto (C_c)^{1/2} \\ C_c = C_5 = 0: & \quad \delta \propto (C_3)^{1/4} \\ C_c = C_3 = 0: & \quad \delta \propto (C_5)^{1/6} \end{aligned} \quad (2a-c)$$

The same dependencies are obtained from a wave-optical theory based on the Contrast Transfer Function (CTF), which quantifies the aberrations of the objective lens. The CTF is given by¹⁵:

$$\begin{aligned} W &= e^{i2\pi\chi} = \cos(2\pi\chi) + i \sin(2\pi\chi) \\ \chi &= \frac{1}{2} C_1 \lambda q^2 + \frac{1}{4} C_3 \lambda^3 q^4 + \frac{1}{6} C_5 \lambda^5 q^6 + \dots \end{aligned} \quad (3a,b)$$

C_1 is the defocus, and q the spatial frequency. The point resolution (i.e. the value of q at the first zero crossing of W , in nm^{-1}) is given by $\text{Im}(W) = 0$ when relative phase shifts in the exit wave function are near-zero (weak-phase object). For a strong-phase object (relative phase shifts around π) or amplitude object (exit wave dominated by structure factor contrast) it is given by¹⁶ $\text{Re}(W) = 0$. With $C_1 = C_5 = 0$ we obtain for weak-phase (eq. 4a) and strong-phase/amplitude (eq. 4b) objects:

$$\sin\left(\frac{\pi}{2} C_3 \lambda^3 q_r^4\right) = 0; \quad \frac{\pi}{2} C_3 \lambda^3 q_r^4 = \pi \quad (4a)$$

$$\cos\left(\frac{\pi}{2}C_3\lambda^3q_r^4\right)=0; \quad \frac{\pi}{2}C_3\lambda^3q_r^4=\frac{\pi}{2} \quad (4b)$$

i.e. $\delta=1/q_r \propto C_3^{1/4}$, the same as eq. (2b). Similarly, when $C_1 = C_3 = 0$, $\delta=1/q_r \propto C_5^{1/6}$, as in eq. (2c). Chromatic aberrations are captured in the envelope function¹⁵:

$$E_c(q) = \exp\left(-\frac{(\pi C_c \lambda q^2)^2}{16 \ln 2} \varepsilon^2\right) \quad (5)$$

Taking $E_c(q_i) = e^{-2}$ to define the information limit¹⁵, the C_c limited resolution is given by:

$$C_c q_i^2 = \frac{4\sqrt{2 \ln(2)}}{\pi \lambda \varepsilon} \quad (6a-b)$$

$$\delta = 1/q_i \propto C_c^{1/2}$$

as in eq. 2a. Thus, eqs.1 and 3 lead to identical results.

Looking at the aberration coefficients individually, with the other coefficients set to zero, for the resolution to reach 50% (10%) of its uncorrected value, C_c must be corrected to better than 25% (1%), C_3 to better than 6.25% (0.01%), and C_5 to better than 1.5% (1 ppm); the window in which the benefits of aberration correction can be obtained shrinks rapidly with increasing order. The stability of the corrected state is determined by the derivatives of resolution with respect to the aberration coefficients. When these derivatives are zero, the system is stable and protected from small fluctuations. However, these derivatives scale with $C_c^{-1/2}, C_3^{-3/4}, C_5^{-5/6}$, diverging as the corrected state is approached. That is, the corrected state is intrinsically unstable, and the more fully it is realized, the more unstable it is.

In the following we use a more realistic and complete scheme of calculating resolution. Using the CTF to calculate images for specific objects¹⁶, all aberration coefficients up to 5th order are set at the actual values calculated for a C_c / C_3 corrected LEEM/PEEM instrument¹⁷. We calculate images at $C_1 = 0$ for amplitude objects¹⁸ as commonly encountered in LEEM, and extract the resolution. We use $\Delta E_0 = 0.25$ eV, and the column energy $E = 15$ keV. Figure 1a shows resolution vs. C_3 (normalized to the uncorrected value) with C_c ranging from uncorrected (100%) to fully corrected (0%). As C_c decreases a deep cusp develops near $C_3 = 0$. The minimum does not reach zero, as higher order coefficients¹⁷ (such as C_{cc} , and C_5) are set at the non-zero values obtained from raytracing. The minimum is shifted to a slightly negative value of C_3 , offsetting the positive value of C_5 . The dotted $\delta \sim C_3^{1/4}$ line is in close agreement with the full calculations when $C_c = 0$. These results do not depend significantly on E_0 . The effects of non-zero defocus will be discussed in more detail below.

In figure 1b $C_3 = 0$ and C_c is varied for different values of E_0 . The dotted line shows $\delta \propto C_c^{1/2}$. For all values of E_0 , as C_c increases the simulations follow $\delta \propto C_c^{1/2}$ closely. Figure 1c compares $\Delta E_0 = 0.25$ eV (cold field emission¹⁹) with $\Delta E_0 = 0.75$ eV (typical LaB₆ gun²⁰). The ordinate is not normalized, to highlight differences on an absolute scale. Dotted lines are individually scaled $\delta \sim C_c^{1/2}$ lines. While near $C_c = 0$ the two cases are almost identical, for the uncorrected situation the difference is significant. As expected, the minimum is steeper and narrower as ΔE_0 increases and chromatic aberration is more

significant. Very similar results were obtained for weak-phase objects¹⁸, or by plotting point resolution (eq. (4)) vs. C_3 for amplitude and weak-phase objects.

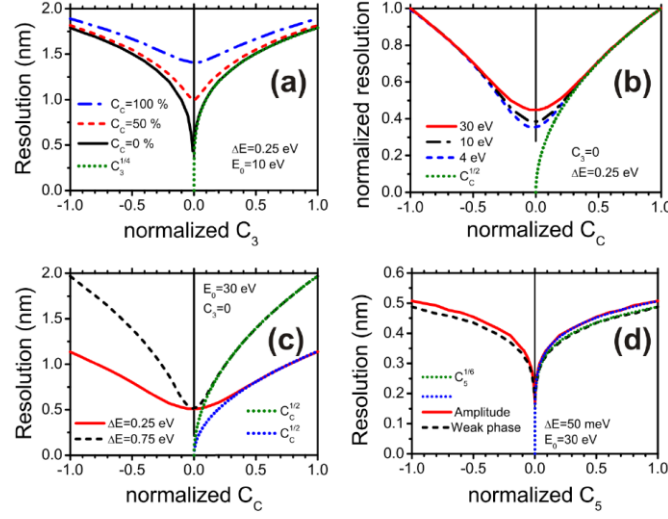


Figure 1. (a) Resolution of an amplitude object vs. the normalized value of C_3 , for different settings of C_c (uncorrected = 100%, fully corrected = 0%). Start energy $E_0 = 10$ eV, $\Delta E_0 = 0.25$ eV. Green dotted line: $C_3^{1/4}$ prediction of eqs. (2b) and (4b). (b) Resolution (normalized to uncorrected values) vs. normalized value of C_c , with $C_3 = 0$, for $E_0 = 4, 10$ and 30 eV. (c) Resolution vs. normalized value of C_c , with $C_3 = 0$, for $\Delta E_0 = 0.25$ and 0.75 eV. Dotted lines in (b) and (c): $C_c^{1/2}$ prediction of eqs. (2a) and (6b). (d) Resolution vs C_5 for C_c / C_3 corrected LEEM with $\Delta E_0 = 50$ meV. The microscope has (near) atomic resolution of 0.17 nm. However, this corrected state is very fragile: a 0.003 excursion from the minimum along the abscissa degrades the resolution by 20%. The dotted lines show the $C_5^{1/6}$ prediction.

Finally, in figure 1d we consider a ‘super-corrected’ LEEM in which $C_c = C_3 = 0$. The remaining chromatic aberrations are minimized by an energy-filtered gun with $\Delta E_0 = 50$ meV. The cusp around $C_5 = 0$ shows the predicted $C_5^{1/6}$ dependence. This microscope promises atomic resolution (0.17 nm) with 30 eV electrons, limited by the higher order chromatic terms. It is conceivable that such an instrument be designed and built, using an electron mirror with at least four electrostatic elements to control C_1, C_3, C_5 and C_c . C_5 must be reduced from 14.5 m to < 0.5 mm¹⁷, C_3 from ~ 300 mm to ~ -10 μm , with a stability of ~ 0.5 μm , and C_1 must be controlled to better than 2 nm. However, the corrected state would be extremely fragile due to the very steep and narrow cusp in figure 1d.

Turning to transmission microscopes, the C_3 -limited TEM resolution at Scherzer defocus is given¹⁵ by $\delta = 0.66 C_3^{1/4} \lambda^{3/4}$, the same $C_3^{1/4}$ dependence as seen before. In the following we focus on the region of slightly negative C_3 and slightly positive C_1 which previous studies have shown to give the highest resolution imaging results. Figure 2a shows the point resolution (the q value at the first zero-crossing of $\sin(2\pi q \chi)$, in nm^{-1}) vs C_3 for a weak-phase object in a TEAM-like microscope² ($C_5 = 5$ mm, 300 keV). We note the presence of a narrow, ridge-shaped optimum-resolution band diagonally across the figure, with optimum performance along the yellow line near the center. The CTF along this line

is optimally balanced over all spatial frequencies below the point resolution and is characterized by a single parameter, $0 < \phi < \pi/2$ (see supplementary material). At $\phi = \pi/2$ figure 2a shows a singularity where two line-shaped singularities intersect.

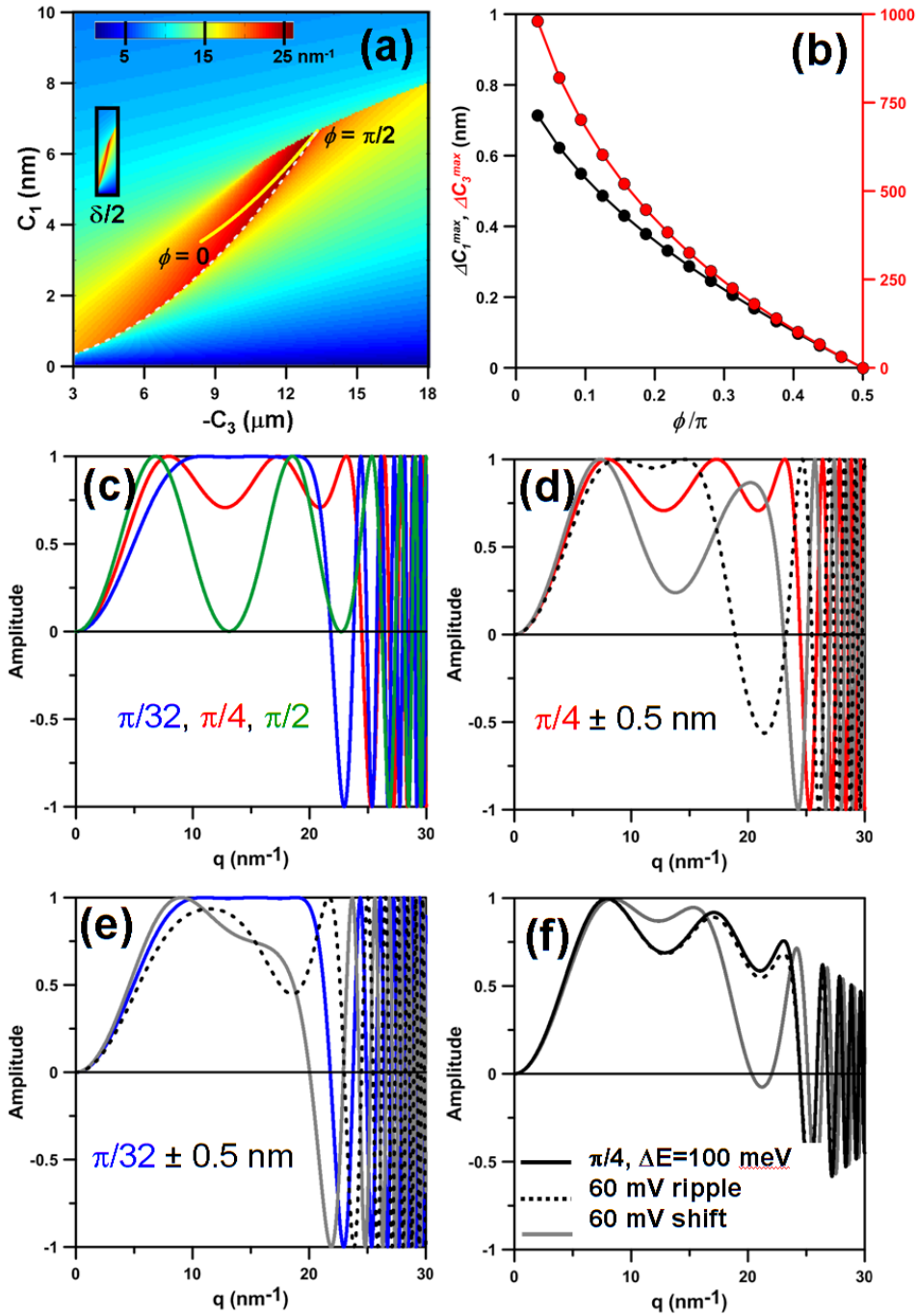


Figure 2. (a) Point resolution (in nm^{-1}) vs C_1 and C_3 near $C_3 = 0$. Yellow line: optimized performance as a function of ϕ , ranging from $\phi = 0$ to $\pi/2$. White dashed line: abrupt instability in the transfer function. The inset below the scale bar, labeled $\delta/2$, shows the relative size of this map if resolution is improved by a factor 2 by reduction of C_5 . (b) Instability budgets for C_1 and C_3 , defined by the distance between the yellow and white-dashed lines in (a), as a function of ϕ . (c) CTF for different values of ϕ . (d) CTF at $\phi = \pi/4$ with

negative (dashed grey) and positive (solid grey) 0.5 nm additional defocus. (e) as (d) for $\phi = \pi/32$. The sensitivity for a small defocus is greater in (d) than in (e), in agreement (b). (f) CTF at $\phi = \pi/4$ with $\Delta E = 100$ meV (black line). Dashed line: additional high voltage ripple $v = 60$ mV. Solid grey line: high voltage shift of -60 mV.

To the right of this point the resolution is always inferior. Along the white dashed line the CTF becomes unstable and the resolution drops abruptly. The distance between the yellow and white lines is the largest deviation that can be tolerated without a significant loss of resolution, defining an ‘instability budget’ for C_1 and C_3 (see supplementary material). Figure 2b plots the instability budgets as a function of ϕ . The budget for C_1 decreases from ~ 0.7 nm at $\phi = \pi/32$ to 0 nm at $\phi = \pi/2$, while for C_3 it changes from ~ 1 μm to 0 μm . At the same time, δ changes from 46 pm at $\phi = \pi/32$ to 38 pm at $\phi = \pi/2$. Note that these instability budgets are not fixed: they depend on the value of ϕ selected by the operator. Figure 2c shows the CTF for $\phi = \pi/32$, $\pi/4$, and $\pi/2$. For $\phi = \pi/4$ (Scherzer defocus) the instability budgets for C_1 and C_3 are ~ 0.28 nm and ~ 0.32 μm , respectively. For $\phi = \pi/32$ resolution is somewhat worse, but stability has improved. In figures 2d and 2e we plot the CTF at $\phi = \pi/4$ (2d) and $\phi = \pi/32$ (2e), with additional offsets in C_1 of ± 0.5 nm, exceeding the instability budget for $\phi = \pi/4$, but well below it for $\phi = \pi/32$. In figure 2d the CTF is strongly affected, with a deep minimum at $q \approx 20$ nm^{-1} for -0.5 nm defocus. The CTF in figure 2e is much less affected, with a point resolution well above 20 nm^{-1} at -0.5 nm defocus, and 20 nm^{-1} at +0.5 nm defocus. This may seem counter-intuitive. To obtain 50 pm resolution, it would appear that the CTF at $\phi = \pi/4$ is better than at $\phi = \pi/32$, as it has a higher point resolution. However, it is also significantly less stable. In practice, one may prefer the small loss in resolution at $\phi = \pi/32$, as it provides a better instability budget. The map in figure 2a is not specific for a TEAM-like instrument. Every electron microscope where C_1 and C_3 can be adjusted for a given C_5 behaves in the same manner. As shown in the supplement, resolution scales with $C_5^{1/6}$, while the instability budgets for C_1 and C_3 scale with $C_5^{1/3}$ and $C_5^{2/3}$, respectively. The advent of C_3 correction led to an improvement in resolution by about a factor 2. Could we gain another factor 2 by reducing C_5 ? The small inset labeled $\delta/2$ in figure 2a shows the relative size of the resolution map resulting from a reduction of C_5 from 5 mm to 0.08 mm, required to improve the resolution by a factor 2. Regardless of the fact that this would present huge, possibly insurmountable challenges in controlling numerous other aberrations, it is clear from the diminutive size of this map that the leading aberrations C_1 and C_3 could not be controlled with sufficient accuracy and stability to make such an improvement possible; the instability budgets have shrunk to near-nothing.

When C_c is corrected the system is -to first order- insensitive to small fluctuations in the electron gun potential. But when only C_3 is corrected, a small shift v in the electron gun potential V is equivalent to a focus shift $\Delta C_1 = C_c \cdot v/V$. To appreciate the difference between a high frequency ripple, vs. a static shift of the gun potential, we refer to figure 2f. We use $C_c = 1.6$ mm, an energy spread $\Delta E = 100$ meV, and no high voltage ripple (solid black line). The slow drop-off for $q > 10$ nm^{-1} is due to the chromatic envelope function, eq. (5). The dashed line results when -in addition to the energy spread of 100 meV- we introduce an additional high voltage ripple of 60 mV. The effect is minor: a

slightly stronger drop-off at higher q -values. In contrast, the grey line uses $\Delta E = 100$ meV, no HV ripple, plus a *static* HV shift of -60 mV, equivalent to $\Delta C_1 = -0.32$ nm. Now the CTF has changed dramatically, and the CTF amplitude at $q = 20 \text{ nm}^{-1}$, critical for a spatial resolution of 50 pm, has dropped to about zero. To keep ΔC_1 stable to within 0.16 nm, the absolute voltage stability (i.e. immunity against drift) must be better than 30 meV at 300 keV (10 meV at 100 keV), a relative stability of 0.1 ppm. When C_c is not corrected, using a gun monochromator²¹ reduces the energy spread *prior* to acceleration to the final beam energy. However, instabilities in the acceleration stage (i.e. drift in the high tension supply for the electron gun) remain unremedied. A similar effect is caused by instabilities in the objective lens current, I : a small current shift i causes a defocus shift $\Delta C_1 = 2C_c \cdot i/I$. Thus, the objective lens power supply must have a relative stability of 5×10^{-8} . Such extraordinary long-term drift stabilities are extremely difficult to realize experimentally. For a TEAM-like instrument, the gun high voltage can drift over 100 mV on a timescale from minutes to hours, depending on the quality of the air conditioning in the room²². Of course, mechanical drift of the sample along the beam direction, as well as undulations in the thin sample foil also give rise to defocus shifts.

These results are not limited to LEEM or TEM, but hold for any electron optical instrument. As more aberration coefficients are corrected, the widths of the cusps within which correction must be maintained become increasingly narrow. Our findings shed new light on the short-lived corrected state observed in state-of-the-art aberration corrected TEM instruments⁹⁻¹¹. With resolution exquisitely sensitive to the residual values of the aberration coefficients, even minute mechanical and electronic drifts are strongly amplified. Uncorrected chromatic aberrations can create a small ‘island of stability’ around the corrected state. Figure 1a shows that this island is reasonably broad when C_c is uncorrected. But when C_c is corrected it shrinks dramatically, leaving the improved corrected state much less protected. Additionally, as the quality of the corrected state is improved it becomes increasingly difficult to reliably put and keep the system into that state. To put the CTF at $\phi = \pi/4$ within 30% of the instability budget, we must measure C_1 and C_3 with sufficient accuracy, and know the value of C_5 to better than 1.5% . When we reduce C_5 , increase in instability outstrips improvement in resolution, posing a fundamental limit on the resolution that is ultimately achievable.

While the intrinsic instability identified in this paper presents a serious challenge, it may be possible to monitor the state of the microscope in real time, and adjust the instrument settings ‘on the fly’ to maintain the corrected condition, much like most aircraft flying today are inherently unstable without sophisticated electronic control systems. Identifying suitable measurable parameters to fully quantify the state of the microscope during routine sample observation is a task that presently remains unresolved.

Acknowledgements: The authors thank Phil Batson for useful discussions. We also thank the referees for their helpful comments. This research was funded in part by the Netherlands Organization for Scientific Research (NWO) via an NWO-Groot Grant (‘ESCHER’).

References

1. P.W. Hawkes, *Biology of the Cell* **93** (2001) 432–439; *Advances in Imaging and Electron Physics; Aberration-corrected Electron Microscopy, Volume 153* (P.W. Hawkes, editor) Academic Press, Amsterdam, 2008
2. C. Kisielowski, et al.; *Microscopy and Microanalysis* **14** (2008) 454; J. C. Meyer, C. Kisielowski, R. Erni, M. D. Rossell, M. F. Crommie, A. Zettl; *Nano Letters*, **8** (2008) 3582
3. R.M. Tromp, J.B. Hannon, A.W. Ellis, W. Wan, A. Berghaus, O. Schaff; *Ultramicroscopy* **110** (2010) 852; Th.Schmidt, et al.; *Ultramicroscopy* **110** (2010) 1358
4. R. Könenkamp, R.C. Word, G.F. Rempfer, T. Dixon, L. Almaraz, T. Jones; *Ultramicroscopy* **110** (2010) 899
5. J. Zach, M. Haider, *Nucl. Instr. Meth.* **A363** (1995) 316
6. S. Itose, M. Matsuya, S. Uno, K. Yamashita, S. Ebata, M. Ishihara, K. Uchino, H. Yurimoto, K. Sakaguchi, M. Kudo; *Microscopy and Microanalysis* **17**, supplement S2, (2011) 654
7. E. Munro, J. Rouse, H. Liu, L. Wang, *J. Vac. Sci. Technol.* **B26** (2008) 2331
8. H.H. Rose, *Phil. Trans. Ro. Soc.* **A36** (2009) 3809
9. J. Barthel, A. Thust; *Ultramicroscopy* **111** (2010) 27
10. J. Biskupek, P. Hartel, M. Haider, U. Kaiser, *Ultramicroscopy*, in press
11. P. Ercius, M. Boese, Th. Duden, U. Dahmen, *Microsc. Microanal.* **18** (2012) 676
12. G. Rempfer; *Journal of Applied Physics* **67** (1990) 6027; G. Rempfer, M.S. Mauck, *Optik* **92** (1992) 3
13. M. Haider, S. Uhlemann, E. Schwan, H. Rose, B. Kabius, K. Urban; *Nature* **392** (1998) 768; O.L. Krivanek, N. Dellby and A.R. Lupini, *Ultramicroscopy* **78** (1999) 1
14. M. Haider, H. Müller, S. Uhlemann, J. Zach, U. Loebau, R. Hoeschen; *Ultramicroscopy* **108** (2008) 167
15. D.B. Williams, C.B. Carter, *Transmission Electron Microscopy: A Textbook for Materials Science*, Second edition, Springer, 2009
16. S.M. Schramm, A.B. Pang, M.S. Altman, R.M. Tromp; *Ultramicroscopy* **115** (2012) 88
17. R.M. Tromp, W. Wan, S.M. Schramm; *Ultramicroscopy* in press, 2011. doi:10.1016/j.ultramic.2011.09.011
18. A.B. Pang, Th. Müller, M.S. Altman, E. Bauer; *Journal of Physics: Condensed Matter* **21** (2009) 314006
19. R.M. Tromp, M. Mankos, M.C. Reuter, A.W. Ellis, M.W. Copel, *Surf. Rev. Lett.* **5** (1998) 1189
20. L.H. Veneklasen *Ultramicroscopy* **36** (1991) 76
21. B. Freitag, S. Kujawa, P.M. Mul, J. Ringnalda, P.C. Tiemeijer, *Ultramicroscopy* **102** (2005) 209; P.C. Tiemeijer, M. Bischoff, B. Freitag, C. Kisielowski, *Ultramicroscopy* **114** (2012) 72; D.C. Bell, C.J. Russo, D.V. Kolmykov, *Ultramicroscopy* **114** (2012) 31
22. P.C. Tiemeijer, private communication.